Frequency dependence of surface acoustic wave swimming

Accepted Version

C. Pouya, K. Hoggard, S. H. Gossage, H. R. Peter, T. Poole and G. R. Nash

College of Engineering, Mathematics and Physical Sciences, University of Exeter, Exeter,

EX4 4QF, UK

Abstract

Surface acoustic waves (SAWs) are elastic waves that can be excited directly on the surface of piezoelectric crystals using a transducer, leading to their exploitation for numerous technological applications, including for microfluidics. Recently the concept of SAW streaming, which underpins SAW microfluidics, was extended to make the first experimental demonstration of "SAW swimming", where instead of moving water droplets on the surface of a device, SAWs are used as a propulsion mechanism. Using theoretical analysis and experiments, we show that the SAW swimming force can be controlled directly by changing the SAW frequency, due to attenuation and changing force distributions within each SAW streaming jet. Additionally, an optimum frequency exists which generates a maximum SAW swimming force. The SAW frequency can therefore be used to control the efficiency and forward force of these SAW swimming devices. The SAW swimming propulsion mechanism also mimics that used by many microorganisms, where propulsion is produced by a cyclic distortion of the body shape. This improved understanding of SAW swimming provides a testbed for exploring the science of microorganism swimming, and could bring new insight to the evolutionary significance for the length and beating frequency of swimming microbial flagella.

Introduction

The properties of surface acoustic waves (SAWs) have been investigated since Lord Rayleigh delivered the first mathematical discussion on the propagation of waves on the free surface of an elastic solid in an address to the London Mathematical Society in 1855 [1]. However, it was the invention of the interdigital transducer (IDT) in 1965 by White and Voltmer [2], allowing SAWs to be directly excited on the surface of piezoelectric crystals, that enabled SAW devices to be developed for applications such as signal processing. Over the last decade, or so, SAW devices have also had a growing presence in the field of microfluidics [3, 4] due to the phenomenon of acoustic streaming [5], where SAWs can be used to induce fluid motion. When a water droplet is applied to the surface of a SAW device, the propagating SAWs are converted into 'leaky SAWs', which are radiated into the liquid and decay, causing fluid motion [5, 6]. This effect can cause droplet formation, vibration and movement as well as ejection of smaller droplets [6, 7]. Applications of acoustic streaming include micro-manipulators for small particles or cells [8], microchannel transport [9], atomization [10, 11], microfluidic-mixing [12], among many others [13].

Very recently, Bourquin and Cooper [14] extended the concept of SAW streaming [6] to present the first, and only reported, experimental demonstration of 'SAW swimming', where instead of moving droplets on the surface of a device, SAWs are used as an aquatic propulsion mechanism for a centimeter scale vessel. In this work we report the first theoretical model of this phenomenon, and use this model to an overlooked property of SAW swimming; the frequency dependence of the swimming force. We show that there is an optimum frequency which generates the maximum force, which we confirm in an experimental study.

Ultimately this improved understanding could lead to the development of artificial swimming devices, with no moving-parts, for applications such as minimally invasive endoscopic surgery. In addition, these results might also help further the understanding of the fundamental science of microorganism swimming, who use similar cyclic movements to propel themselves.
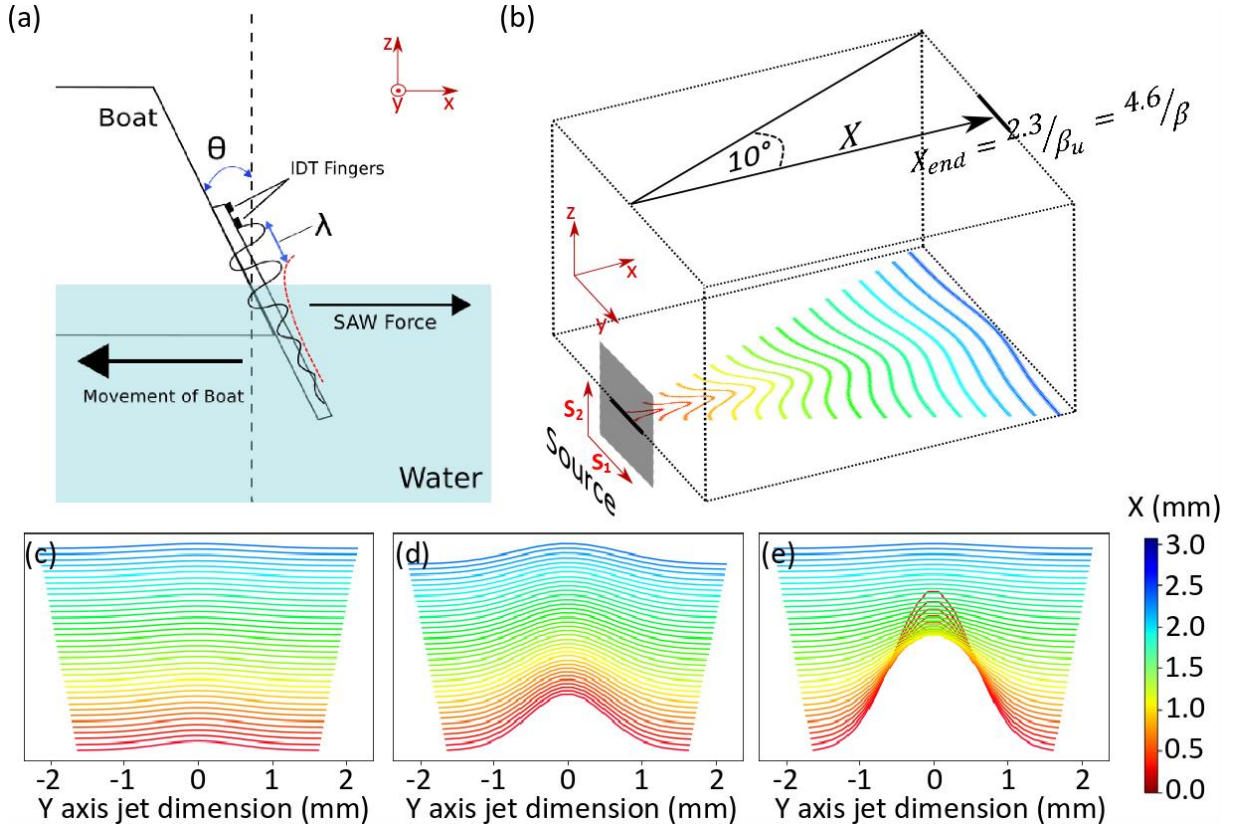
Figure 1. SAW swimming device and jet arrangement (a) Schematic of the boat design and SAW swimming phenomenon, showing the SAW exponentially decaying (red dotted line) as it hits the water and turns into a leaky SAW, producing a SAW streaming force from the rear of the boat and driving the vessel forwards. λ is the SAW wavelength $=2d$, where d is determined by the separation between fingers of the IDT. The fundamental frequency of the IDT is 11 MHz. (b) Schematic of the jet emitted from the SAW source with Gaussian beam divergence and edge of jet definitions from Dentry et al. [16]. Also shown are axes of the source dimension co-ordinates s_1 and s_2 (relating to L_1 and L_2). (c-e) Off-axial profiles are shown as a set of Gaussians scaled by an axial force profile taken from the main image in figure 2b. Gaussian force profiles across the jet close to the source (<3 mm) are shown for clarity (c) below the peak frequency (11 MHz), (d) around the peak frequency (56 MHz) and (e) above the peak frequency (146 MHz).

Results

Theoretical Analysis and Discussion

The frequency dependence of the SAW streaming force was identified by performing an in-depth study of the leaky SAW jet profile in di-ionised (DI) water. The theoretical physics describing the velocity produced by SAW streaming was discussed in-depth by Lighthill [15] with alterations to this theory in a recent paper by Dentry et al. [16] which thoroughly analysed the axial jet velocity profile of a SAW

streaming jet produced from a configuration similar to the SAW swimming system presented here. Dentry et al. fixed a SAW device in place and the SAW device was positioned at an angle of theta=0°, so that the SAW streaming force was not directed parallel to the surface of the water. In our study the device is free to move and is positioned at the Rayleigh angle of 23° [14], as shown schematically in figure 1a, to allow the vessel to produce a maximum force in the direction of propulsion. The Rayleigh angle is given by

$$\theta_R = \sin^{-1} \frac{v_F}{v_{SAW}}. \tag{1}$$

Here v_F is the velocity of the longitudinal wave in the fluid, and v_{SAW} is the velocity of the SAW. Although Dentry et al. perform an in depth analysis of velocity profiles within SAW streaming jets, Lighthill [15] and Dentry et al. [16] also briefly discuss the equations governing SAW streaming forces within the jet. We extend the analysis performed by Lighthill [15] and Dentry et al. [16] to analyse force distributions within SAW streaming jets and from this we determine the theoretical thrust of a SAW swimming device. The jet emanates from the source and follows an axial jet trajectory along X as shown in figure 1b. Perpendicular to this, the jet's velocity and force profiles are assumed to follow a Gaussian distribution and undergo a spreading, emanating from the source. The purely axial velocity and force density profiles for each frequency are described by equation 2 and 3 below [16]:

$$u(X, s_1, s_2) = \sqrt{\frac{2f(X)}{\pi S_1(X)S_2(X)}} \tag{2}$$

$$F(X, s_1, s_2) = \frac{\rho f'(X)}{\pi K_1(X)K_2(X)} \tag{3}$$

where u is the jet velocity and S is related to the beam spread in the dimension of the reference frame of the source, perpendicular to X. s_1 and s_2 are the axes of the source. S and K describe the spread of the jet at a position X across the length of the jet. For our study we assume $S_i(X)$ and $K_i(X)$ to be equal to the radius of an almost conical jet at each point along X in the coordinates perpendicular to the axial jet profile. S at each point along X is determined by the finite source width (the interdigital transducer (IDT) aperture $L_1 = 3.25$ mm) and the beam spread with semiangle of 10° [16]. The length of the device submerged in the water was taken as the same length $L_y = 3.25$ mm, for all frequencies representing a typical submerged length during SAW swimming experiments (total length of an experimental device = 5.4 mm). Therefore, the projection of this at 23° [16] was taken as the source dimension in the second

5

dimension L_2 to account for the Rayleigh angle. Finite source dimensions and beam spread were included due to the analysis performed by Dentry et al. [16], who verified experimentally that the inclusion of a finite source dimension to Lighthill's model [15] allowed accurate theoretical analysis to be made of velocity profiles within the jet. Dentry et al. also showed that a beam spread with semiangle of approximately 10° was consistent for all analysed frequencies from 19.7 to 936 MHz over a range of powers. A schematic of this is shown in figure 1b. F is the acoustic body force per unit volume and ρ is the density of the liquid (998 kgm^{-3}). $f(X)$ is related to the total momentum flux across the jet cross-section at constant X and is described by

$$f(X) = \frac{1}{\rho c}P[1 - e^{-\beta X}] \tag{4}$$

Where c is the speed of sound in the liquid (1498 ms^{-1}), β is the attenuation coefficient of the beam power $\beta = 2\beta_u = \frac{\frac{4}{3}(\mu+\mu')\omega^2}{\rho c^3}$ [16], where μ is the shear viscosity of the fluid (10^{-3} Pa s), μ' represents the bulk viscosity of the fluid (taken as 2.47 x 10^{-3} Pa s, [17]) and ω is angular frequency. Therefore the attenuation coefficient of the beam power β is frequency-dependent. $f'(X)$ is the spatial derivative of $f(X)$. P is the total power of the sound beam, which is related to the power at the source, and decays along the substrate when the SAW is in contact with the fluid due to attenuation [16]. When in the water, the power along the substrate decays as $e^{-2\alpha y}$ [16] where α is the SAW attenuation coefficient = $\frac{\rho c}{\rho_s V_{SAW}\lambda_{SAW}}$, ρ_s is the density of the substrate and λ_{SAW} is the SAW wavelength. The total power was considered as the integral of this power decay [16] across the device from 0 to L_y (the submerged second source dimension) multiplied by an original power P_0 before the SAW is in contact with the fluid (taken as an estimate of $P_0 = 25$ mW as a typical input power expected from experiments) (i.e. $P = P_0 \int_0^{Ly} e^{-2\alpha y}dy$ where y is the distance travelled along the substrate which has been adapted from the power decay equation $P = \int_0^\infty \rho wc\dot{\eta}_m^2 e^{-2\alpha y}dy$ from Dentry et al. [16], where w is the width of the wavefront and $\dot{\eta}_m$ is the vibrational velocity before contact with a fluid). The SAW attenuation coefficient α describes the wavelength-dependent, and therefore frequency-dependent, attenuation across the substrate, the second frequency dependent attenuation in the system. These variables are all constituent variables in the velocity equation (equation 2) and force equation (equation 3). In turn, this

6

results in a highly frequency dependent velocity equation (equation 2) and force equation (equation 3). Perpendicular to the axial direction, the jet's velocity and force profiles exhibit a Gaussian distribution, with the maximum velocity or force positioned at the axial position within the jet. As such, the force and velocity profiles across the length at off-axis points across the jet width have a similar form but with reduced absolute values as given by Dentry et al. [16] (i.e. $u(X, s_1, s_2) = \sqrt{\frac{2f(X)}{\pi S_1(X)S_2(X)}} \exp\left[-\left(\frac{s_1}{S_1}\right)^2 -\left(\frac{s_2}{S_2}\right)^2\right]$ and $F(X, s_1, s_2) = \frac{\rho f'(X)}{\pi K_1(X)K_2(X)} \exp\left[-\left(\frac{s_1}{K_1}\right)^2 - \left(\frac{s_2}{K_2}\right)^2\right]$). Here, to simplify the model, we consider only axial velocities and forces.

The axial velocity profile of jets with SAW frequencies in an experimentally accessible range were calculated using equation 2 and are plotted in figure 2a. The distributions are shown clearly at positions within the jet close to the source, as shown in figure 2a and b where velocity profiles are plotted up to a maximum of 15 mm. Figure 2a shows that the peak velocity increases and its position moves closer to the source with increasing frequency, consistent with previous studies [16]. The beam length, considered by Dentry et al. [16] to end when the power is reduced to 1% of the initial power is reduced to a smaller length with increasing frequency (figure 2b inset and supporting information table S1). The end of the beam, i.e. position within the jet where the power is reduced to 1% of the power at the source, P, can be shown to be located at $X_{end} = \frac{2.3}{\beta_u} = \frac{4.6}{\beta}$ and therefore proportional to $\frac{1}{\omega^2}$ (figure 1b and supporting information table S1) [16]. The peak velocity is presented in figure S1 and the differences between our study and Dentry et al is likely to arise due to the differences in our models including the different values of L_1, L_2 and L_y used. Previous studies [16, 18] have analysed the peak velocity for different frequency jets, yet none have analysed the frequency dependence on force.
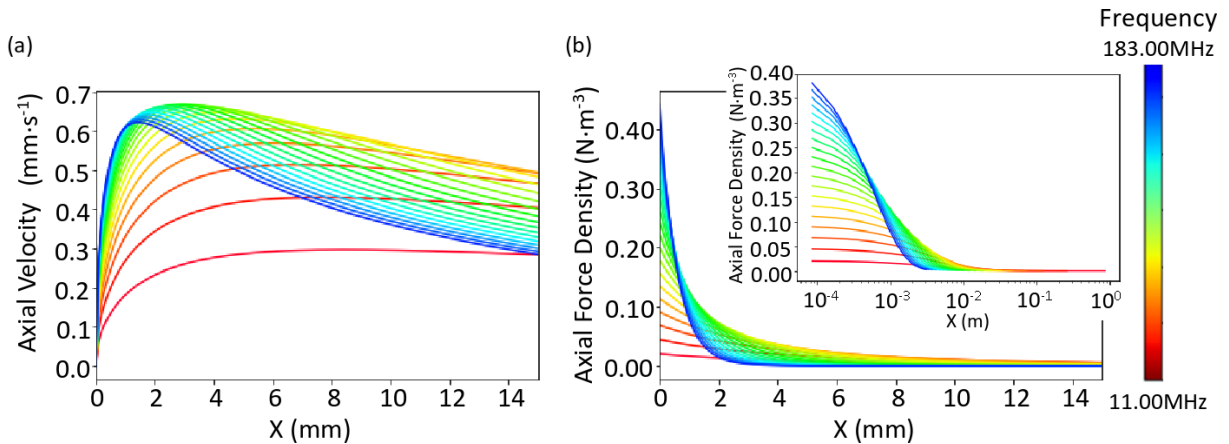
Figure 2. Calculated velocity and force profiles (a) Axial velocity profile (across *X*) within the jet calculated by equation 2 with 20 different SAW input frequencies close to the source (<15 mm) measured in linear steps from 11 to 183 MHz. (b) Axial force per unit volume profile close to the source (<15 mm) calculated by equation 3 for 20 different SAW input frequencies and (inset) until the edge of the jet where the power reaches 1% of the initial value.

The axial force density of 20 different jets with SAW frequencies within an experimentally accessible frequency range were calculated from equation 3 (figure 2b). Figure 2b shows the force distributions of all frequency jets within an axial distance close to the source (<15 mm) and the inset shows the whole length of each profile until the end of the jet where the power reaches 1% of the power at the source. Each force profile, for each frequency, was integrated over the distance *X* from the source until its associated 1% jet edge, using the Python numpy.trapz package function. The results are plotted in figure 3, which show that there is a maximum axial force at a SAW frequency of approximately 56 MHz. Additionally, we also adapt the theoretical model to consider total jet lengths that are not limited to above 1% of the initial power. Figure 3 also shows the integrated axial forces calculated using two standard jet lengths for all frequencies within the confines of a container, one with standard length of 40 cm (the maximum length of the water container used in the experiments and presented in a later section) and one smaller size of 1 cm to represent a theoretical minimum possible jet length within a container. The differences in the force profiles for jet lengths considered within a finite domain and up to the 1% jet edge are minimal (figure 3). For the 1 cm jets, only the lower frequency axial forces decrease slightly when compared to the 1% power jets.

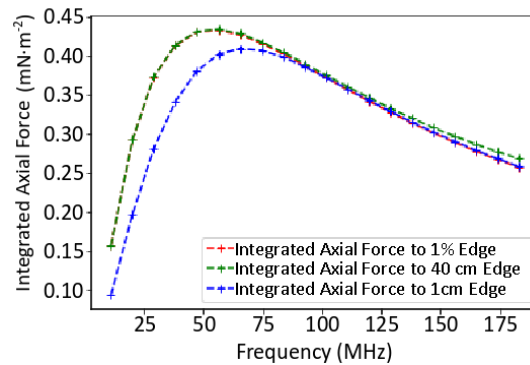**Figure 3.** The axial force calculated from equation 3, and integrated across *X* up to the edge of the jet for 20 different SAW input frequencies. The edge of the jet was considered to be when the jet power reaches 1% of the source power with attenuation length dependence varying as $1/_{\omega^2}$ (red curve), we also consider two standard jet lengths within the confines of a finite container with standard length of

40 cm (green curve) and 1 cm (blue curve) for all frequencies. The red curve tends to that of the green curve at lower frequencies and to the blue curve at higher frequencies.

For the 40 cm jets, there is a small increase in the axial force at higher frequencies where highly attenuated forces from beyond the 1% jet edge are now included in the jet calculations. A slight difference in the absolute axial force values exist at lower and higher frequencies when considering constant finite jet lengths for all frequencies, but a peak force is still present with a slight shift in its frequency. The physical origin of the peak force can be understood by interpretation of the force profiles in figure 2b and by analysing the redistribution of forces within each jet with respect to the change in SAW input frequency. The key to changing forces within each jet arises from 2 frequency-dependent attenuations; the attenuation of the jet within the water (with β dependence) and the atenuation of the power along the substrate (with α dependence). Analysis of force profiles show that lower SAW input frequencies produce a steadier small axial force with gradual changes throughout the long jet length. As the SAW input frequency is increased, the axial force close to the source increases. Additionally, with increasing frequency, attenuation greatly reduces the length of the jet comprising substantial forces and so forces close to the source contribute significantly to the total axial force. The maximum force close to the source increases linearly with frequency, while the attenuation of jet length is proportional to $1/{\omega^2}$, However, each frequency has its own force expression which incorporates these factors, and is a combination of α (frequency dependent SAW attenuation coefficient), β (the frequency dependent attenuation coefficient of the beam power) and exponentials of these terms (all of which are frequency dependent) which produces a unique curve shape/force profile for each frequency jet. There exists an optimum frequency, where the initial axial force is high and the force profile is such that larger forces are maintained for longer distance, but attenuation of the jet is not considerable, resulting in larger axial forces over longer distances. Beyond this frequency, attenuation of the jet reduces the jet lengths comprising substantial forces and so the total axial force at higher frequencies is significantly reduced. When changing frequency, the balance of increasing forces close to the source and the changing force distributions due to the two frequency-dependent attenuations of the jet give rise to a changing total integrated axial force and a peak in the axial force at around 56 MHz.

9

As non-axial forces are represented by the axial force scaled by a Gaussian, a schematic representation of the axial force close to the source (<3 mm) within the jet of a frequency below the peak frequency (11 MHz), around the peak frequency (56 MHz) and above the peak frequency (146 MHz) are shown in figure 1 c, d and e, respectively. It is apparent from the Gaussian representation that attenuation produces higher forces (peaks in figure 1c-e) close to the source, over shorter distances when frequency is increased, but attenuation means these forces are only present over short distances. Comparatively, the lower frequency representation (figure 1c) shows low forces and the optimum frequency (figure 1d) has consistently larger forces over longer distances.

Experimental Results and Discussion

To validate the experimental setup, which consisted of a SAW device mounted on a polystyrene vessel, the net forward force resulting from the SAW force was first measured as a function of SAW power at a SAW frequency of 11MHz, as shown in figure S2. The measured swimming force increases approximately linearly with increasing SAW power, in agreement with theory (Equation 3 and 4) and previous experiments [14]. The size of the measured SAW swimming force is also consistent with the maximum value, 8mN, obtained by Bourquin and Cooper [14] at a SAW frequency of ~11 MHz, transducer aperture of 15mm, and an acoustic power of 1.7W. In our case, we obtain a value of the SAW swimming force 0.04 mN at 11 MHz, but for a transducer aperture of 3.25 mm, and an estimated acoustic power of approximately 25 mW (taking into account the transmission coefficient of the IDTs and other losses in the system). Correcting for these factors, would give a maximum SAW swimming force of 12 mN.

To investigate the frequency dependence of the SAW swimming force, a second SAW device was mounted onto a boat of the same design. In this case the RF signal was pulsed (period of approximately 1.5s) to prevent excessive heating of the SAW device [14]. The acoustic power was approximately 25mW. The movement of the boat was then measured at 5 different input frequencies: 11, 32, 97, 119 and 183 MHz and the net forward forces resulting from SAW forces were calculated at 0.5s after the application of the RF signal, at each frequency. The measured force, corrected for the frequency response of the system and normalised to the fundamental frequency response of the IDT, is plotted as

function of frequency in figure 4 and shows a strong non-linear dependence on the SAW (note that due to the discrete resonances of the IDTs, values of the force could not be obtained at frequencies between 32MHz and 97MHz). For comparison, values of the swimming force calculated from theory are also plotted in Figure 4. Overall, there is good agreement between the frequency dependence of the measured and calculated forces. The difference in the measured and calculated values of the force, with the calculated forces approximately half of the measured forces, is because only axial forces were considered in the theoretical calculation. As the jet spreads away from the axial line, the force distributions are reported to be the same [15, 16] with smaller absolute values, represented by a Gaussian distribution. Therefore it is practical that the theoretical force distribution at off-axial angles will simply increase in absolute values when these off-axial forces are also considered.
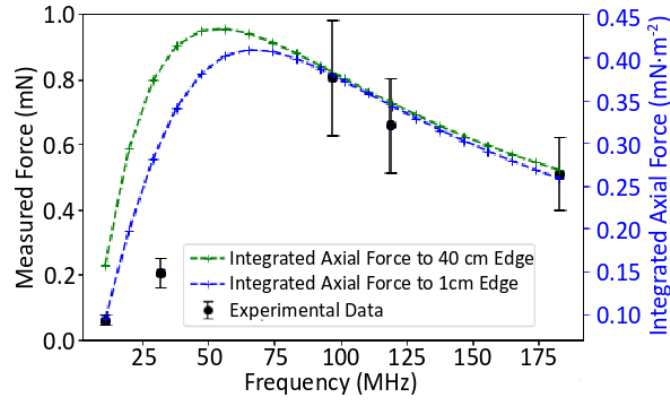

Figure 4. The experimental SAW forces measured over the time period of 0.5 s at 5 resonant input frequencies of the SAW device (11, 32, 97, 119 and 183 MHz), normalised by systematic errors from the experimental setup including the transmission coefficient of the IDTs. Also shown are the theoretical integrated axial force calculated from equation 3 and integrated across X up to a jet length of 40 cm and 1 cm for 20 different SAW input frequencies spanning the frequency range used in the experiment. Error bars calculated from combined error equation.

Additionally, the theory assumes that the SAW source is static, whereas in the experiments the vessel is moving. This is likely to produce a more complicated beam profile, due to interference, and could change the properties of the SAW swimming efficiency. Movement may also slightly alter the length of the submerged region of the device, giving rise to slightly changing input powers due to the changing source dimension L_y, which could alter the force distribution slightly (see figure S3). Further work is therefore underway to extend the theoretical analysis to include the effects of a moving vessel, and to undertake new experiments using SAW devices designed specifically for SAW swimming. It should be noted that

the frequency at which there is a peak swimming force is likely to vary between different experimental configurations. Finally, the use of a substrate with a slower SAW velocity, such as glass, would allow the development of swimming devices that produce the maximum thrust when they lie almost parallel to the surface of the fluid. This will reduce their macroscopic drag, but will also remove the requirement for the SAW device to be mounted on a centimetre size vessel. In this case, the SAWs could also be excited remotely using a laser [19].

Conclusion

We theoretically predict and experimentally observe the presence of an optimum frequency for a SAW swimming device which gives rise to a maximum net forward force or thrust when placed in water. The value of the optimum frequency is reliant on the frequency-dependent attenuating properties of the surrounding fluid. For our experimental study, the optimum frequency lies between 32 and 97 MHz, but it should be noted that this frequency is likely to vary between different experimental configurations. Our experimental study is consistent with the results we obtained from a theoretical model which shows that the peak force for this device arises at a frequency of ~56 MHz, and that the force profiles within the jet have very different distributions at different frequencies. The main differences result from attenuations of the jet which consequently change the absolute values of axial force across the jet which dramatically alters the total axial forces. This improved understanding, at a fundamental level, of this phenomenon, provides a foundation on which to design devices with improved performance and functionality. It could underpin future work to develop swimming devices with no moving parts, for applications such as minimally invasive endoscopic surgery. In addition, the use of multiple SAW frequencies, with different induced forces, could allow precise control of fluids in lab-on-a-chip applications, including SAW sorters [20]. Recent studies [21, 22] have altered IDT geometries and substrates in order to add additional frequency control to their SAW streaming systems, additional alterations to the system could allow additional frequency control to a SAW streaming system.

Finally, it is interesting to note that the phenomenon of SAW swimming mirrors the propulsion mechanism of many microorganisms, such as bacteria, who move to find food, shelter and escape predators. Microorganisms have evolved methods of movement to overcome and exploit drag, in their low Reynolds number environment, where propulsion is produced by a cyclic distortion of their body

12

shape [23-25], with similar wavelengths to that of the SAWs used here [23-27]. Some hypothesise that SAW motion and acoustic streaming is a likely propulsion method for some bacteria [28]. Different swimming strategies include using cilia and flagella, or by small multicellular organisms [25]. In many cases the technological design of medical micro-robotics are inspired by, or similar to, swimming microorganisms [29]. For instance the spiral micro-robot designed by Ishiyama et al. [30], which is similar to some cilium propulsion mechanisms, or the artificial bacteria flagella [31, 32] which use magnetics to induce motion. In addition to magnetic propulsion, a recent review [29] highlighted other methods of medical micro-robotic propulsion including 'propulsion by bubbles', 'propulsion by chemical reaction' and 'propulsion by biological mechanism' as methods of propulsion for medical swimmers. The experimental investigation of micro-swimming is challenging due to the difficulty in controlling the relevant key parameters, such as the wavelength of the cyclic distortion. Using SAWs, we have shown that there is a frequency/wavelength dependence of the force produced by a similar cyclic motion, which if it exists for flagella locomotion could pose an evolutionary significance relating the beating frequency, wavelength or length of flagella to producing an optimum or more efficient force. If so, an optimum beating frequency, or length, of the flagella of individual swimmers could also be tailored to their native fluid environment, which might possess specific attenuating or viscosity properties. SAW swimming devices can therefore be used as a test-bed to allow greater insight into the science underlying microorganism movement.

Materials and Methods

To test these results, the frequency response of a SAW swimming device was measured experimentally. A commercially available 128° YX LiNbO3 SAW delay line, with a centre-to-centre IDT separation distance of 5.4 mm and IDT aperture of 3.25 mm, was mounted on a printed circuit board (PCB) using conductive silver epoxy and 25μm diameter bond wires. The IDTs had a double-digit geometry, allowing the efficient excitation of SAWs at a number of discrete resonant frequencies. The SAW wavelength λ_{SAW} =2d, where d is determined by the separation between fingers of the IDT. The fundamental frequency of the IDT is 11 MHz. To form the swimming device, the PCB was mounted onto the rear of a polystyrene vessel using non-porous adhesive carbon tape, dimensions 40mm x 25

13

mm x 30 mm (length, height and width respectively) and mass 2.3460 $\pm$ 0.0005 g (figure 1a). The swimming device was placed in a container, dimensions 0.4m $\times$ 0.4m $\times$ 0.1m, filled with several cm DI water and free to move whilst under test. The rear of the boat was sculpted at an angle of 23° to the vertical axis to allow the SAWs to refract into the water and to propagate parallel to the surface of the water [8], as defined by the Rayleigh angle, given by equation 1. The device was positioned to account for the Rayleigh angle of the refracted SAW, so that the SAW streaming force was directed parallel to the surface of the water, resulting in the vessel being propelled in the opposite direction. Movement of the vessel was induced by exciting SAWs at the input transducer of the device using a connected Hewlett-Packard 8648C RF signal generator, the output from which was amplified using a Mini-circuits TVA-R5-13A amplifier. The displacement of the vessel over a defined period of time (0.5 s), from the application of the RF signal, was recorded using a GoPro Hero4 Silver camera at a rate of 60 frames per second. The time interval of 0.5 s was chosen as it was found to minimise the effects of the drag and resistive forces, arising from the surrounding water and the restoring force of the connecting wires, on the measurement of the force.

From the recorded data, the acceleration of the vessel was calculated using the equations of motion ($a = \frac{2s}{t^2}$ where a is the acceleration of the vessel and s is the distance travelled in time t.) and the net forward force resulting from the SAW force was calculated using Newton's 2nd law. This is the resultant forward force from the SAW force, reduced by drag forces from the surrounding water and the mechanical resistance experienced due to tethering from the connecting cables.

Author Contributions

G. R. N. conceived the study and guided the experiments and theoretical modelling; C. P. performed the theoretical modelling and analysis; K. H., S. H. G., H. R. P. and T. P. fabricated samples and performed experiments; C. P. and G. R. N. wrote the manuscript with contributions from all authors.

Data Accessibility

All data supporting this study is provided in the results section of the paper or as supplementary information accompanying this paper.

Funding Statement

References

[1] Lord Rayleigh, *On waves propagated along the s-plane of and elastic solid,* Proc. London Math. Soc. **17**, 4, (1885).

[2] R. M. White and F. M. Voltmer, *Direct piezoelectric coupling to surface elastic waves*. Appl. Phys. Lett. **7**, 314, (1965).

[3] J. Friend and L. Y. Yeo, *Microscale acoustofluidics: microfluidics driven via acoustics and ultrasonics,* Rev. Mod. Phys. **83**, 647, (2011).

[4] X. Ding at al., *Surface acoustic wave microfluidics,* Lab Chip **13**, 3626, (2013).

[5] W. Nyborg, *Physical Acoustics edited by W. P. Mason 2B*, (Academic Press, New York, 1966), pp. 265-331.

[6] S. Shiokawa, Y. Matsui, and T. Moriizumi, *Experimental study on liquid streaming by SAW*, Jpn. J. Appl. Phys. **28**:Suppl. 28-1, 126, (1989).

[7] S. Shiokawa, Y. Matsui, and T. Ueda, *Liquid streaming and droplet formation caused by leaky Rayleigh waves*. Proc. Ultrasonics Symposium **641**, 643, (1989).

[8] T. Franke, S. Braunmüller, L. Schmid, A. Wixforth and D. A. Weitz, *Surface acoustic wave actuated cell sorting*, Lab Chip **10**, 789, (2010).

[9] M. Cecchini, S. Girardo, D. Pisignano, R. Cingolani and F. Beltram, *Acoustic-counterflow microfluidics by surface acoustic waves*, Appl. Phys. Lett. **92**, 104103 (2008).

[10] M. Kurosawa, T. Watanabe, A. Futami and T. Higuchi, *Surface acoustic wave atomizer*, Sens. Actuators A **50**, 69, (1995).

[11] K. Chono, N. Shimizu, Y. Matsui, J. Kondoh and S. Shiokawa, *Development of novel atomization system based on SAW streaming*, J. Appl. Phys. **43**, 2987, (2004).

[12] T. Frommelt, M. Kostur, M. Schäfer, P. Talkner, P. Hänggi and A. Wixforth, *Microfluidic mixing via acoustically driven chaotic advection*, Phys. Rev. Lett. **100**, 034502, (2008).

[13] L. Y. Yeo and J. R. Friend, *Surface Acoustic Wave Microfluidics*, Annu. Rev. Fluid Mech. **46**, 379, (2014).

[14] Y. Bourquin and J. M. Cooper, *Swimming using surface acoustic waves*. PLoS ONE **8**, (2013).

[15] J. Lighthill, *Acoustic streaming*. J. Sound Vib. **61**, 391, (1978).

[16] M. B. Dentry, L. Y. Yeo, and J. R. Friend, *Frequency effects on the scale and behavior of acoustic streaming*. Phys. Rev. E **89**, 013203, (2014).

[17] M. J. Holmes, N. G. Parker, and M. J. W. Povey, *Temperature dependence of bulk viscosity in water using acoustic spectroscopy*. J. Phys.: Conf. Ser. **269**, 012011, (2011).

[18] B. Tiller, J. Reboud, M. Tassieri, R. Wilson, and J. M. Cooper, *Frequency dependence of microflows upon acoustic interactions with fluids*, Physics of Fluids 29, 122008, (2017).

[19] A. Harata, H. Nishimura, and T. Sawada, *Laser-induced surface acoustic waves and photothermal surface gratings generated by crossing two pulsed laser beams*. Appl. Phys. Lett. **57**, 132, (1990).

[20] T. Huang, C. E. Cameron, J. P. McCoy, L. Wang, S-C. S. Lin, M. I. Lapsley, Y. Chen, F. Guo, S. Li and Xiaoyun Ding, *An On-Chip, Multichannel Droplet Sorter Using Standing Surface Acoustic Waves*. Anal. Chem. **85**, 5468, (2013).

[21] Y. Bourquin, J. Reboud, R. Wilson and J. M. Cooper, *Tuneable surface acoustic waves for fluid and particle manipulations on disposable chips.* Lab Chip **10**, 1898, (2010).

[22] Y. Bourquin, R. Wilson, Y. Zhang, J. Reboud and J. M. Cooper, *Phononic Crystals for Shaping Fluids*, Adv. Mater. **23**, 1458, (2011).

[23] S. Vogel, *Life in Moving Fluids* (Princeton University Press, New Jersey, 1996).

[24] E. Lauga and T. R. Powers, *The hydrodynamics of swimming microorganisms*. Rep. Prog. Phys. **72**, 096601, (2009).

[25] J. Elgeti, R. G. Winkler, and G. Gompper, *Physics of microswimmers—single particle motion and collective behavior: a review*. Rep. Prog. Phys. **78**, 056601, (2015).

[26] Sir G. Taylor, *Analysis of the swimming of microscopic organisms*. Proc. R. Soc. Lond. A **209**, 447, (1951).

[27] H. A. Stone and A. D. T. Samuel, *Propulsion of microorganisms by surface distortions.* Phys. Rev. Lett. **77**, 4102, (1996).

[28] K. M. Ehlers and J. Koiller, *Could cell membranes produce acoustic streaming? Making the case for Synechococcus self-propulsion*. Mathematical and Computer Modelling **53**, 1489, (2011).

[29] J. Feng and S. K. Cho, *Mini and Micro Propulsion for Medical Swimmers*. Micromachines 5, 97, (2014).

[30] K. Ishiyama, K. I. Arai, M. Sendoh, and A. Yamazaki, *Spiral-Type Micro-Machine for Medical Applications*. Proceedings of the 2000 International Symposium on Micromechatronics and Human Science, Nagoya, Japan, 22–25 October 2000; pp. 65–69.

[31] L. Zhang, J. J. Abbott, L. Dong, B. E. Kratochvil, D. Bell, B. J. Nelson, *Artificial bacterial flagella: Fabrication and magnetic control*. Appl. Phys. Lett. **94**, 064107, (2009).

[32] D. J. Bell, S. Leutenegger, K. M. Hammar, L. X. Dong, B. J. Nelson, *Flagella-Like Propulsion for Microrobots Using a Nanocoil and a Rotating Electromagnetic Field*. Proceedings of the 2007 IEEE International Conference on Robotics and Automation, Roma, Italy, 10–14 April 2007; pp. 1128–1133.